When are Quantum Algorithms Applicable for Signal Decoding in Wireless Communication?

ABDULMOHSEN ALSAUI (Member, IEEE), IBRAHIM AL-NAHHAL (Senior Member, IEEE), AND OCTAVIA A. DOBRE (Fellow, IEEE)

Faculty of Engineering and Applied Science, Memorial University of Newfoundland, St. John's, NL A1B 3X5, Canada

CORRESPONDING AUTHOR: A. ALSAUI (e-mail: aamalsaui@mun.ca)

This work was supported in part by the Canada Research Chair Program under Grant CRC-2022-00187, and in part by the Canada First Research Excellence Fund under Grant CFREF-2022-00062.

ABSTRACT Multiple-input multiple-output (MIMO) technology utilizes multiple antennas at the transmitter and receiver to enhance data transmission speeds and reliability. Traditional MIMO decoding methods, however, can become increasingly complex as the number of antennas and modulation order rises. Quantum computing brings forth a new realm of information processing with significant potential. This study investigates the applicability of quantum algorithms for decoding information in MIMO wireless communication systems. Specifically, the Dürr-Høyer quantum search, based on Grover's algorithm, and optimal quantum sorting algorithms are leveraged to reduce the query complexity with an analysis of the complexity and achievable bit error rate performance of the quantum-assisted decoders. The study considers cases of MIMO diversity, spatial modulation, and multiplexing transmission using both maximum-likelihood and fixed-complexity sphere decoders. By examining a variety of communication scenarios, this work aims to assess the applicability of quantum algorithms across different operational regimes and aids in extending the methodology to other communication systems.

INDEX TERMS Dürr-Høyer (DH) algorithm, fixed-complexity sphere decoder (FCSD), Grover's algorithm, maximum-likelihood (ML) decoder, multiple-input multiple-output (MIMO) communication, quantum algorithm, quantum computing, wireless communication.

I. INTRODUCTION

IN THE rapidly advancing domain of wireless communications, multiple-input multiple-output (MIMO) technology plays a pivotal role in supporting the upcoming demands of 6G networks [1], [2], [3]. MIMO systems significantly enhance transmission speeds and reliability by employing multiple antennas at both the transmitter (Tx) and receiver (Rx) ends [4]. Moreover, they can be utilized in different forms depending on the desired quality-of-service. For example, adding redundancy by transmitting the same signal across all Tx antennas has the benefit of increased reliability and range, referred to as spatial diversity scheme [4], [5]. When higher data rates are desired, the spatial multiplexing scheme is employed to transmit independent data streams across each Tx antenna, which is more prone to channel interference than the diversity scheme [4], [6]. Another possible variant is the spatial modulation scheme, where the Tx antenna selection is used to encode part of the input data besides the transmitted modulated signal. Limiting the concurrent usage of Tx antennas reduces the required radio frequency (RF) chain/hardware while achieving a performance between the diversity and multiplexing schemes [7], [8].

In general, the holy grail of communication systems is to attain a reliable, error-free, and high-rate data transfer. For that, signal detection is essential. With the inevitable existence of non-ideal channel conditions, the maximum-likelihood (ML) decoder achieves the optimal uncoded performance [9]. Although being the optimal decoder, ML is impractical in many use cases as it incurs an immense decoding complexity. A practical alternative is the fixed-complexity sphere decoder (FCSD), which allows tuning the decoding complexity depending on the target performance. Despite the algorithmic and technological advancements,

decoding signals in MIMO systems remains a significant challenge due to the high complexity demands, particularly as the number of Tx antennas and modulation orders increases. The demand to push the boundaries of current capabilities prompts the need for groundbreaking technologies, such as machine learning and quantum computing [10], [11].

The main idea behind quantum computing is to make use of systems exhibiting quantum mechanical properties for information processing. Although a universal fault-tolerant quantum computer has yet to be realized, it is essential to fully understand its capabilities and potential to prepare for its eventual arrival. Researchers have actively worked on developing quantum algorithms that can outperform their classical counterparts. Recently, it has been established that quantum computing provides an unparalleled computational advantage for certain algorithmic problems, such as solving large systems of linear equations and optimization tasks [12], [13]. A significant application of quantum computers is breaking encryption schemes that depend on large numbers factorization by using Shor's quantum algorithm [14]. Wireless communication has also benefited from this new computing paradigm, with quantum algorithms simulated on classical computers proving feasible for a range of problems, including signal detection, error-correction, resource allocation, channel estimation, and indoor localization [15], [16], [17], [18]. In a practical setting, a quantum computer would need to be located in a central processing unit, such as in the cloud, due to its high cost and significant size, weight, and power requirements.

The computational speedup of quantum computers has attracted researchers to explore its application to signal detection within wireless communications [19], [20], [21], [22], [23], [24]. Quantum search algorithms (QSAs) offer significant reductions in query complexity compared to classical methods. In [19], variants of the Dürr-Høyer (DH) and Boyer-Brassard-Høyer-Tapp (BBHT) QSAs were applied to a MIMO orthogonal frequency division multiplexing system, demonstrating notable improvements in detection performance compared to traditional QSAs. Reduced complexity and enhanced performance are showcased by [20], which utilized a quantum version of the repeated weighted boosting search algorithm for channel estimation and multi-user signal detection in a MIMO system. The applicability of QSA-assisted particle swarm optimization for non-orthogonal multiple access systems is analyzed in [21], highlighting its potential in optimizing resource allocation and user signal detection. Furthermore, [22] studied the performance of a multi-carrier interleave-division multiple-access system, showcasing significant performance gains. Application of the DH QSA for a multi-user MIMO system is presented in [23] and [24], where the potential for reduced complexity is demonstrated. The discussed literature work only employed QSAs for the ML decoder. More practical decoders, like FCSD, have yet to be investigated. Moreover, focusing on specific systems limits the potential to generalize how well QSAs can perform across different systems and operational regimes.

Given that quantum computing has proven beneficial in specific ML signal detection problems, a critical question arises: when are quantum algorithms applicable for signal decoding in wireless communication? This study aims to answer the question by employing the most effective quantum algorithms for database searching and sorting. For that, three system models (i.e., diversity, spatial modulation, and multiplexing) are considered with two decoders (i.e., ML and FCSD), answering the raised question with respect to the achieved complexity and performance. In summary, the contributions of this paper are as follows:

1) A comprehensive analysis of the ML and FCSD algorithms' working principles, complexity, and performance was provided for a MIMO system with diversity, spatial modulation, and multiplexing transmission schemes. Notably, novel FCSD algorithms were introduced specifically for the diversity and spatial modulation schemes.
2) Mathematically derived the number of real multiplications (RM), real additions (RA), and query complexities, providing a comprehensive and fair set of complexity measures for the investigated decoders and transmission schemes.
3) Examined the operational principles, constraints, and performance capabilities of relevant quantum algorithms, determining their exact probability of success and complexity as a function of the database size, using Monte Carlo simulations to estimate these metrics.
4) Bridged the gap between quantum computing capabilities and the practical needs of signal decoding in wireless communication systems by evaluating the potential for applying quantum algorithms across diverse wireless communication systems, taking into account their unique algorithmic requirements and search space scales.
5) Analyzed the performance of the quantum-assisted ML decoder across the three transmission schemes, with spatial modulation introduced as a novel consideration.
6) For the first time, integrated quantum algorithms with the FCSD algorithm across diversity, spatial modulation, and multiplexing schemes.
7) Conducted a thorough analysis of the considered systems, rigorously testing various settings to highlight the limitations of quantum algorithms, including the use of Monte Carlo simulations to model system behavior under uncertainty.

The ultimate goal of this work is to evaluate the potential of quantum computing in advancing the efficiency and reliability of signal detection in next-generation wireless communications.

The paper is structured to first delve into the fundamentals of the considered MIMO communication systems in Section II, followed by an overview of the ML and FCSD

classical decoding methods and their usage in Section III. Then, Section IV gives an introduction to the principles of quantum mechanics relevant to quantum computing. The working principle and capability of relevant quantum algorithms are discussed in Section V. After that, Section VI presents the performance of the quantum-assisted decoders, assessing the implications of utilizing quantum algorithms for signal detection in MIMO systems. Finally, Section VII concludes the deduced concepts and generalizations from the obtained performance.

Notation: Vectors and matrices are denoted by boldfaced lowercase and uppercase letters, respectively. The space of $a \times b$ complex matrices is denoted by $\mathbb{C}^{a\times b}$. The transpose and complex conjugate transpose operations are denoted by $(\cdot)^T$ and $(\cdot)^\dagger$, respectively. The cardinality of a set and the Euclidean norm of a vector are represented by $|\cdot|$ and $\|\cdot\|$, respectively. $\lfloor\cdot\rfloor$ and $\lceil\cdot\rceil$ denote the floor and ceiling functions, respectively. The imaginary unit is represented by $i = \sqrt{-1}$. Finally, $\otimes$ denotes the tensor product.

II. SYSTEM MODEL

In this section, the investigated MIMO system and its operational scenarios are described. With N_t Tx antennas, the different operational schemes vary based on the nature of the transmitted signal

$$\mathbf{x} = \begin{cases} \begin{bmatrix} x & x & \cdots & x \end{bmatrix}^T & \text{Spatial Diversity,} \\ \begin{bmatrix} 0 & \cdots & x_j & \cdots & 0 \end{bmatrix}^T & \text{Spatial Modulation,} \\ \begin{bmatrix} x_1 & x_2 & \cdots & x_{N_t} \end{bmatrix}^T & \text{Spatial Multiplexing,} \end{cases} \quad (1)$$

where $\mathbf{x} \in \mathbb{C}^{N_t\times 1}$ and x_j is the symbol transmitted from the j^{th} antenna. For the diversity scheme, the same symbol is transmitted by all antennas. The redundancy aids in combating the non-ideal channel conditions [4], [5]. On the other hand, unique symbols are transmitted in the multiplexing scheme, enhancing the system data rate [4], [6]. In spatial modulation, a single Tx antenna is activated, reducing the need for additional RF chains hardware [7], [25]. Fig. 1 depicts the three considered transmission schemes. After transmission, the signal is affected by fading and additive white Gaussian noise (AWGN). For N_r Rx antennas, the received signal, $\mathbf{y} \in \mathbb{C}^{N_r\times 1}$, is given by

$$\mathbf{y} = \mathbf{H}\mathbf{x} + \mathbf{n}, \quad (2)$$

where $\mathbf{H} \in \mathbb{C}^{N_r\times N_t}$ is the channel matrix representing the Rayleigh fading and $\mathbf{n} \in \mathbb{C}^{N_r\times 1}$ is the AWGN vector whose elements have zero-mean and variance σ^2.

III. CLASSICAL DECODERS

When the signal is received, decoders are employed to retrieve the transmitted signal, $\mathbf{x}$. The channel state information is assumed to be perfectly known at the Rx. This section introduces the theoretically optimal ML decoder and the more practical FCSD algorithm, elaborating on their decoding methodology and algorithmic complexity.

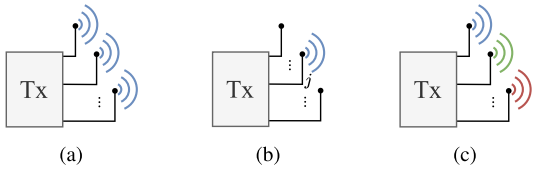

FIGURE 1. Illustrations of the (a) diversity, (b) spatial modulation, and (c) multiplexing communication schemes.

A. MAXIMUM-LIKELIHOOD (ML) DECODER

The ML decoder is the most powerful decoding technique for retrieving an uncoded transmitted signal. It operates by comparing the received signal to all possible transmitted signals, $\mathcal{P}$, and selecting the one that is most likely to have been transmitted. For a modulation order M, the cardinality of the possible transmission space depends on the utilized scheme

$$|\mathcal{P}| = \begin{cases} M & \text{Diversity,} \\ MN_t & \text{Spatial Modulation,} \\ M^{N_t} & \text{Multiplexing.} \end{cases} \quad (3)$$

The decoding process involves calculating the likelihood of each candidate signal and choosing the one that maximizes this likelihood. The decoded symbols are given by

$$\tilde{\mathbf{x}}_{\text{ML}} = \underset{\mathbf{x}\in\mathcal{P}}{\operatorname{argmin}} \|\mathbf{y} - \mathbf{H}\mathbf{x}\|^2. \quad (4)$$

Since the entirety of the transmission space, $\mathcal{P}$, is considered, the ML algorithm is the optimal decoder in the sense that it minimizes the probability of error [9]. However, ML decoding is impractical for some use cases due to its immense complexity requirement. Instead, complexity-aware decoders, such as the FCSD, are utilized.

B. FIXED-COMPLEXITY SPHERE DECODER (FCSD)

The FCSD is considered a practical alternative to the ML decoder. The rationale behind the FCSD algorithm is to limit the search space, thereby reducing the computational complexity. The considered subspace can be visualized as a circle centered at the received signal, $\mathbf{y}$, with a radius of ρ, giving the decoded symbols as [26]

$$\tilde{\mathbf{x}}_{\text{SD}} = \underset{\mathbf{x}\in\mathcal{P}}{\operatorname{argmin}} \|\mathbf{y} - \mathbf{H}\mathbf{x}\|^2 \quad \text{s.t.} \quad \|\mathbf{y} - \mathbf{H}\mathbf{x}\|^2 \le \rho^2, \quad (5)$$

where ρ acts as a threshold. Fixing the threshold, ρ, results in a variable complexity. On the other hand, allowing it to be varied enables a fixed-complexity operation [27].

In practice, a tree structure is utilized to limit the search space in the FCSD algorithm, which is a graphical representation of (4). For the diversity and spatial modulation schemes, where the symbols do not interfere, the tree resembles a matrix. In this scenario, each tree level (i.e., row) represents the signal received by a specific Rx antenna, while the tree branches (i.e., columns) correspond to different transmission scenarios. Specifically, the i^{th} tree level represents the received signal from the i^{th} Rx antenna.

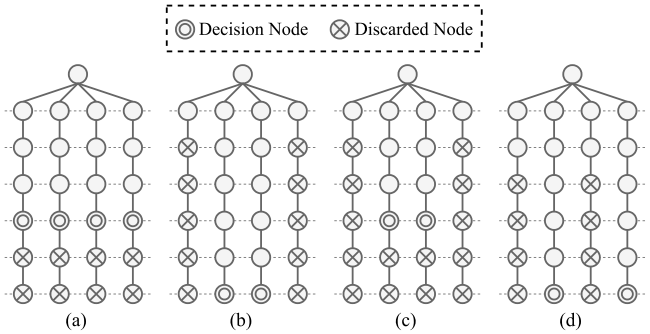

FIGURE 2. Considered tree search algorithms for the diversity ($M = 4$) and spatial modulation ($M = N_t = 2$) schemes: (a) RB with $R = 4$, (b) CB with $C = 2$, (c) CRB with $[C, R] = [2, 4]$, and (d) RCB with $[R, C] = [2, 2]$.

On the other hand, the k^{th} tree branch indicates that the k^{th} and $[(k-1) \bmod M + 1]^{\text{th}}$ symbols were transmitted for the diversity and spatial modulation schemes, respectively [28]. The error associated with a specific tree node (i.e., matrix element) is

$$e_{ik} = |y_i - h_{ik}x_k|^2. \tag{6}$$

To determine the most likely transmission scenario, the accumulated error for each branch is calculated by summing the errors of its constituent tree nodes. Exploring all the tree nodes results in the ML solution. To reduce the complexity of the ML decoder, a two-stage searching strategy is employed to discard some tree nodes. First, a subset of the nodes is used to evaluate the best (i.e., smallest error in (6)) C branches, which are then expanded. Subsequently, the optimal branch is determined by calculating the accumulated error up to the decision node at the end of these expanded branches.

Fig. 2 illustrates the search algorithms utilized for the diversity and spatial modulation schemes, which ignore some tree levels, branches, or a combination of both. The utilized algorithms are: R-best (RB), which considers R rows; C-best (CB), which fully expands the best C branches using only the first row; CR-best (CRB), which expands the best C branches up to the R^{th} row using only the first row; and RC-best (RCB), which fully expands the best C branches using the first R rows. For instance, when $R = C = 2$ for the RCB algorithm in Fig. 2 (d), the accumulated error up to the second tree level determines which two branches will be expanded. The decoded symbol expressions for the aforementioned algorithms are

$$\tilde{\mathbf{x}}_{\text{RB}} = \underset{\mathbf{x}\in\mathcal{P}}{\text{argmin}} \sum_{n=1}^{R} |y_n - \mathbf{h}_n\mathbf{x}|^2, \tag{7}$$

$$\tilde{\mathbf{x}}_{\text{CB}} = \underset{\mathbf{x}\in\mathcal{S}_{\text{CB}}}{\text{argmin}} \|\mathbf{y} - \mathbf{H}\mathbf{x}\|^2, \tag{8}$$

$$\tilde{\mathbf{x}}_{\text{CRB}} = \underset{\mathbf{x}\in\mathcal{S}_{\text{CRB}}}{\text{argmin}} \sum_{n=1}^{R} |y_n - \mathbf{h}_n\mathbf{x}|^2, \tag{9}$$

$$\tilde{\mathbf{x}}_{\text{RCB}} = \underset{\mathbf{x}\in\mathcal{S}_{\text{RCB}}}{\text{argmin}} \|\mathbf{y} - \mathbf{H}\mathbf{x}\|^2, \tag{10}$$

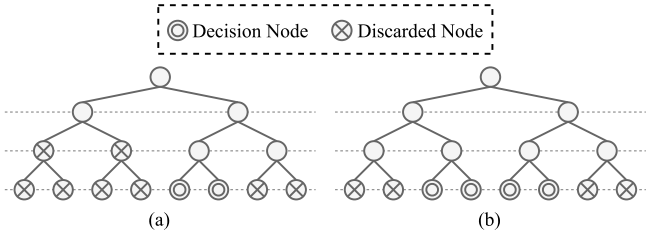

FIGURE 3. Multiplexing tree search with $M = 2$ for (a) $K = 1$ and (b) $K = 2$. Aside from the first level, MK nodes are probed in each level.

where $y_n \in \mathbb{C}^{1\times 1}$ is the n^{th} element of $\mathbf{y}$, $\mathbf{h}_n \in \mathbb{C}^{1\times N_t}$ is the n^{th} row of $\mathbf{H}$, and $\mathcal{S}$ is the limited search space for a given algorithm.

In the multiplexing scheme, unique symbols are simultaneously transmitted, resulting in co-channel interference. Thus, a different tree structure is utilized. First, the QR decomposition of $\mathbf{H}$ is obtained, which gives $\mathbf{H} = \mathbf{QR}$, where $\mathbf{Q} \in \mathbb{C}^{N_r\times N_t}$ is a unitary matrix ($\mathbf{Q}^\dagger = \mathbf{Q}^{-1}$) and $\mathbf{R} \in \mathbb{C}^{N_t\times N_t}$ is an upper-triangular matrix. Multiplying the left-hand side of (5) by $\mathbf{Q}^\dagger$ results in the detected symbols being

$$\tilde{\mathbf{x}}_{\text{KB}} = \underset{\mathbf{x}\in\mathcal{S}_{\text{KB}}}{\text{argmin}} \left\| \begin{bmatrix} z_1 \\ z_2 \\ \vdots \\ z_{N_t} \end{bmatrix} - \begin{bmatrix} r_{11} & r_{12} & \cdots & r_{1N_t} \\ 0 & r_{22} & \cdots & r_{2N_t} \\ \vdots & \vdots & \ddots & \vdots \\ 0 & 0 & \cdots & r_{N_tN_t} \end{bmatrix} \begin{bmatrix} x_1 \\ x_2 \\ \vdots \\ x_{N_t} \end{bmatrix} \right\|^2, \tag{11}$$

where z and r are elements of the vector $\mathbf{z} = \mathbf{Q}^\dagger\mathbf{y}$ and matrix $\mathbf{R}$, respectively, and $\mathcal{S}_{\text{KB}}$ is the search subspace lying in the sphere with radius ρ. In the multiplexing scheme tree, which is depicted in Fig. 3, symbols are recursively detected starting from the last Tx antenna (i.e., x_{N_t}) [29]. Each node is expanded into M possible nodes for the subsequent symbol, resulting in M^{N_t} nodes at the end of the tree. When all the nodes are explored, this results in the ML solution. In practice, the K-best (KB) decoder is used, which expands only the K nodes with the smallest errors at each level. For example, considering $M = K = 2$ as in Fig. 3, a maximum of $MK = 4$ nodes are kept in every level.

C. COMPLEXITY MEASURES

Beyond assessing the error performance achievable by a decoder, it is crucial to consider the involved complexity cost. To comprehensively evaluate a decoder, the following complexity measures are employed:

- *Computational* complexity, which quantifies the RM and RA required to execute a specific algorithm.
- *Query* complexity, $\mathcal{Q}$, which measures the number of times a black-box algorithm is utilized [30]. This depends on information extraction rather than computational effort and is relevant to algorithms that gain

TABLE 1. The computational complexity of the ML decoder for different transmission schemes.

Scheme	RM	RA
Diversity	$6MN_r$	$M[2N_r(N_t+2)-1]$
Spatial Modulation	$2MN_t(N_r+2)$	$MN_t[2(N_t+N_r)+1]$
Multiplexing	$M^{N_t}[2N_r(2N_t+1)]$	$M^{N_t}[2N_r(2N_t+1)-1]$

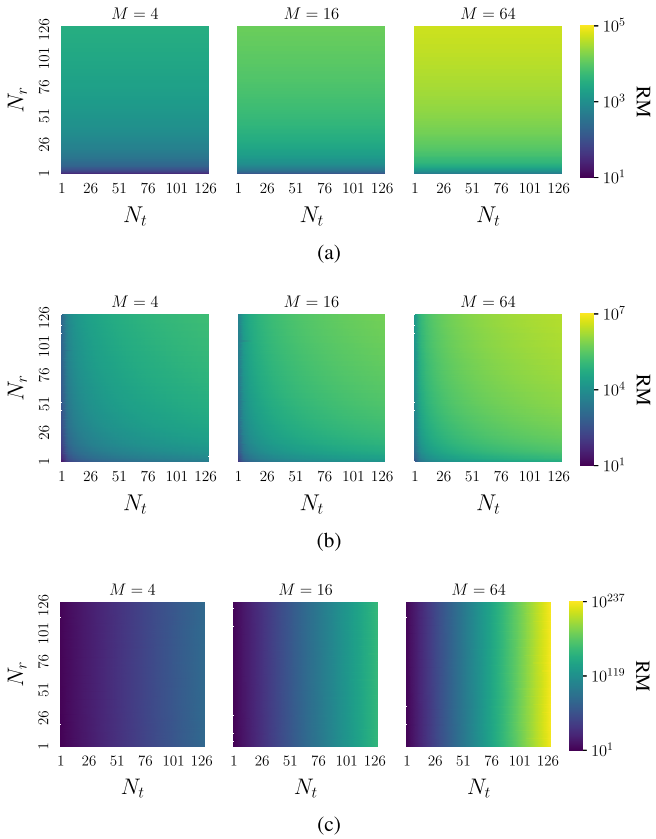

FIGURE 4. The ML decoder RM as a function of the number of Tx and Rx antennas considering different modulation orders, M, for the (a) diversity, (b) spatial modulation, and (c) multiplexing transmission schemes.

information by querying an *oracle*.[1] In the context of minimum element finding and sorting algorithms, query complexity is quantified by the number of comparison operations performed.

The remainder of this subsection is dedicated to deriving and presenting the complexity expressions (i.e., RM, RA, and $\mathcal{Q}$) for the two decoders (i.e., ML and FCSD) under the considered three transmission schemes (i.e., diversity, spatial modulation, and multiplexing). The computational complexity for the ML decoder and FCSD will be derived from (4) and (7)−(11), respectively. For brevity, only the RM will be shown in the figures, while the expressions for both are presented.

[1] An oracle is a black-box operation that encapsulates a specific function that maps inputs to outputs in a desired manner without worrying about the implementation details [31].

For the ML decoder, evaluation of (4) for each possibility $\mathbf{x} \in \mathcal{P}$ entails a computational complexity that depends on the utilized transmission scheme. In the diversity scheme, x can be factored out as can be noted from (3), which results in a relatively low computational complexity of RM $= 6N_r$ and RA $= 2N_r(N_t+2)-1$. For the spatial modulation scheme, with $\mathbf{x}$ having a single non-zero element, the necessary calculations are also simplified, which give RM $= 2(N_r+2)$ and RA $= 2(N_t+N_r)+1$. The multiplexing scheme has the highest computational complexity as the transmitted symbols are independent, resulting in RM $= 2N_r(2N_t+1)$ and RA $= 2N_r(2N_t+1)-1$. Each transmission possibility has an associated fixed computational complexity, so each expression is multiplied by the corresponding value for $|\mathcal{P}|$ from (3). The computational complexity expressions of the ML decoder for all the communication schemes are summarized in Table 1. On the other hand, the query complexity is given by (3), which is the number of possibilities from which to determine the minimum.

The RM as a function of the antenna count is shown in Fig. 4. N_r does not significantly increase the computational complexity in all cases. In contrast, the computational complexity of the multiplexing scheme scales exponentially with N_t. On the other hand, the RM for the diversity scheme is entirely unaffected, as noted in Table 1. It is evident that the computational complexity of the multiplexing scheme becomes excessive for high modulation orders and a large number of antennas.

In the FCSD algorithm, the computational complexity of the diversity and spatial modulation schemes are obtained using the ML decoder expression by replacing N_r and $|\mathcal{P}|$ with R and C, respectively. Except for the single-stage RB algorithm, the two-stage searching strategy can be thought of as two independent ML solutions, with the total computational complexity being their sum. In the multiplexing scheme, the first tree level has M nodes, which require $4M$ RM and RA. For the remaining N_t-2 levels, each node in the n^{th} level entails $4nK$ and $2(n+1)K$ RM and RA, respectively. The computational complexity expressions of the FCSD algorithm are shown in Table 2, where $K \leq M^2$ is assumed for the multiplexing scheme tree.

Fig. 5 and Fig. 6 show the RM of the tree search methods utilized in the diversity and spatial modulation schemes. Increasing the number of tree levels (branches) through the parameter R (C) results in a higher computational complexity. Fig. 7 shows the RM for the KB multiplexing tree algorithm. Increasing M and K results in a constant factor increase in RM, while a higher N_t leads to a much greater RM. Compared to Fig. 4, the FCSD algorithms significantly reduce the computational complexity.

The query complexity of FCSD has two stages: 1) tree expansion and 2) minimum node determination. In the first stage, the nodes with the least error are determined, which requires a sorting algorithm. In the second step, the optimal node is chosen with the query complexity being C for the CB, CRB, and RCB algorithms that are

TABLE 2. Computational complexity of the FCSD algorithm.

Scheme	Algorithm	RM	RA
Diversity	RB	$6MR$	$M[2R(N_t+2)-1]$
	CB	$6(M+CN_r)$	$M[2(N_t+2)-1]+C[2N_r(N_t+2)-1]$
	CRB	$6(M+CR)$	$M[2(N_t+2)-1]+C[2R(N_t+2)-1]$
	RCB	$6(MR+CN_r)$	$M[2R(N_t+2)-1]+C[2N_r(N_t+2)-1]$
Spatial Modulation	RB	$2MN_t(R+2)$	$MN_t[2(N_t+R)+1]$
	CB	$2N_t[3M+C(N_r+2)]$	$N_t\{M[2N_t+3]+C[2(N_t+N_r)+1]\}$
	CRB	$2N_t[3M+C(R+2)]$	$N_t\{M[2N_t+3]+C[2(N_t+R)+1]\}$
	RCB	$2N_t[M(R+2)+C(N_r+2)]$	$N_t\{M[2(N_t+R)+1]+C[2(N_t+N_r)+1]\}$
Multiplexing	KB	$4M\left(1+K\sum_{n=2}^{N_t-1}n\right)$	$2M\left[2+K\sum_{n=2}^{N_t-1}(n+1)\right]$

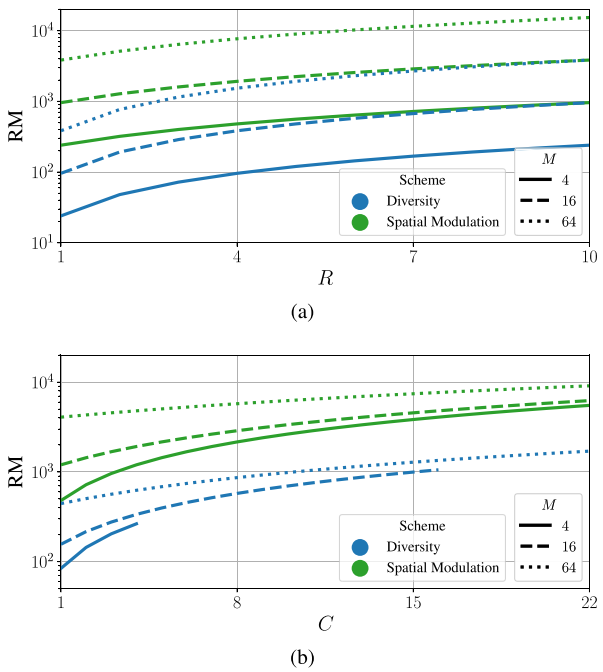

FIGURE 5. The RM dependence on the (a) RB and (b) CB tree search algorithms parameters with $N_t = N_r = 10$.

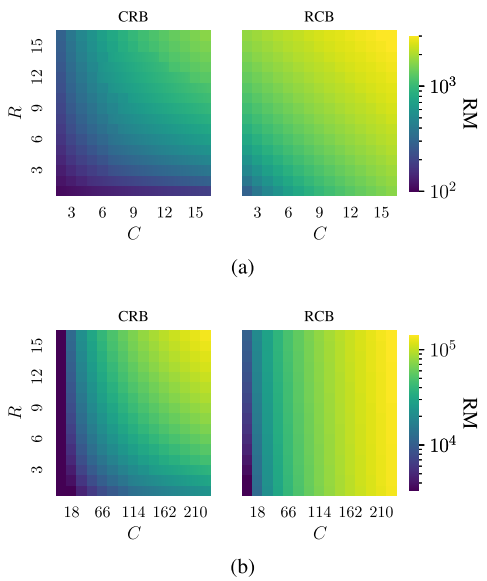

FIGURE 6. The RM considering $M = N_t = N_r = 16$ for the (a) diversity and (b) spatial modulation schemes with the CRB and RCB algorithms.

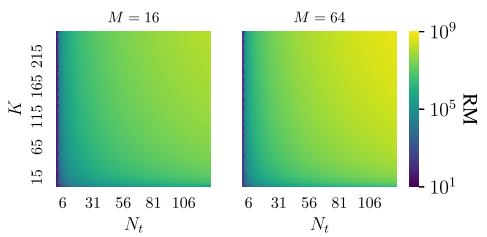

FIGURE 7. The RM as a function of the number of Tx antennas and parameter K, considering different modulation orders for the KB algorithm.

associated with the diversity and spatial modulation schemes. For the RB method, the query complexity for determining the minimum node at the end is identical to the ML decoder case. Tree expansion is performed only once for diversity and spatial modulation trees. In contrast, $N_t - 1$ tree expansions are required for the multiplexing tree. For N nodes, the best sorting algorithms (both classical and quantum) require $O(N\log_2(N))$ compare-and-swap operations [32], [33], which are counted towards the query complexity [30]. However, full sorting is not necessary; partial sorting is sufficient for the FCSD algorithms. In general, to find the smallest k elements, the most efficient classical partial sorting algorithm has a query complexity of $O(N\log_2(k))$ [34]. Thus, the total query complexity of each method for the FCSD algorithm is

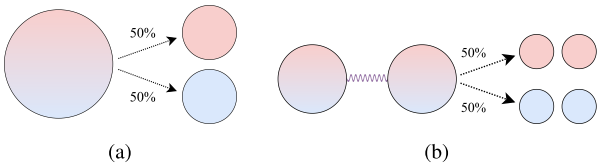

FIGURE 8. Outcome uncertainty for a (a) superposition and (b) entangled states.

$$\mathcal{Q} = \begin{cases} |\mathcal{P}| - 1 & \text{RB}, \\ O\big(|\mathcal{P}| \log_2(C)\big) + C - 1 & \text{CB/CRB/RCB}, \\ O\big(KM \log_2(K)\big) & \\ \quad \times \big(N_t - \lfloor \log_M(K) \rfloor - 1\big) & \\ +KM - 1 & \text{KB}, \end{cases} \tag{12}$$

where $K \geq M$ is assumed. When $K < M$, an extra factor of $O(M \log_2(K))$ is added to the KB method query complexity expression.

IV. QUANTUM COMPUTING

Having highlighted the complexity cost of the considered communication schemes and decoders, there is a desire to reduce these costs. Quantum computing, with its new realm of information processing, offers a potential solution by reducing query complexity. This section covers the basic principles of quantum computing, including an intuition for the quantum advantage, mathematical formalism, and computational problems that can be accelerated.

INTRODUCTORY PRINCIPLES

Classical computers operate using bits, representing 0 or 1. While powerful, it faces challenges for specific computational problems [35]. In addition, classical computing, driven by Moore's Law, faces a bottleneck as chips approach the atomic scale, encountering disruptive quantum phenomena [36]. A quantum bit (qubit) is the fundamental unit of quantum information, capable of existing in multiple states simultaneously, known as *superposition* [37]. Another unique property is *entanglement*, which allows qubits to be correlated in ways not possible in classical computers [38]. Fig. 8 illustrates the uncertainty associated with the two quantum phenomena. In the bra–ket (also known as Dirac) notation, a qubit in a superposition state of both logical bits is represented by

$$|\psi\rangle = \alpha\,|0\rangle + \beta\,|1\rangle\,, \tag{13}$$

where $\alpha, \beta \in \mathbb{C}$ and the utilized computational basis is

$$|0\rangle = \begin{bmatrix} 1 & 0 \end{bmatrix}^T, \quad |1\rangle = \begin{bmatrix} 0 & 1 \end{bmatrix}^T. \tag{14}$$

The magnitude of the complex number represents the qubit's probability of being in some logical state. Thus, the normalization condition $|\alpha|^2 + |\beta|^2 = 1$ holds.

Geometrically, a qubit can be depicted using the Bloch sphere shown in Fig. 9 by re-expressing (13) in terms of the polar, θ, and azimuthal, ϕ, angles as

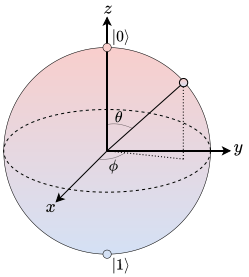

FIGURE 9. Bloch sphere representation for a qubit in a superposition state.

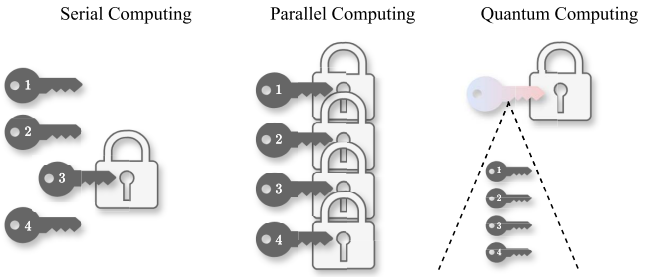

FIGURE 10. Probing of the possibilities for different computing paradigms [24].

TABLE 3. Time and resource efficiencies for the computing paradigms.

	Time Efficiency	Resource Efficiency
Serial Computing	Low	High
Parallel Computing	High	Low
Quantum Computing	High	High

$$|\psi\rangle = \cos\left(\frac{\theta}{2}\right)|0\rangle + e^{i\phi}\sin\left(\frac{\theta}{2}\right)|1\rangle\,, \tag{15}$$

where $0 \leq \theta \leq \pi$ and $0 \leq \phi \leq 2\pi$. The advantage of quantum computing stems from the fact that qubits enable quantum parallelism, which allows for simultaneous probing of possibilities [13]. Fig. 10 illustrates the intuition behind the quantum advantage compared to other paradigms of computing, with the efficiency comparison shown in Table 3. In serial computing, a single computing unit sequentially explores possibilities. While this method is resource-efficient, it is relatively time-consuming. In contrast, parallel computing simultaneously explores possibilities using multiple computing units, significantly reducing the required time. Both advantages can be realized with a quantum computer, where a single unit can explore all possibilities simultaneously. It is important to note that quantum algorithms offer significant speedup only for some computational problems [39], some of which are tabulated in Table 4 along with the associated complexity [13]. Unlike the database search problem, which reduces the query complexity, the quantum advantage in problems like the integer factorization and Fourier transform lies in the significant reduction of computational complexity.

TABLE 4. Complexity comparison of quantum and best classical algorithms for various computational problems.

Problem	Classical Complexity	Quantum Complexity
N-size Database Search	$O(N)$ *Brute Force*	$O\left(\sqrt{N}\right)$ *Grover's*
n-bit Integer Factorization	$2^{O\left(n^{1/3}\right)}$ *Number Field Sieve*	$O(n^3)$ *Shor's*
N-size Fourier Transform	$O(N\log_2 N)$	$O((\log_2 N)^2)$

V. QUANTUM ALGORITHMS

Quantum computing can be leveraged to enhance the capability of searching in an unsorted database, which has many applications in wireless communication [17]. The optimal algorithm to find a particular element, α_d, in a sorted database of size N is the classical binary search algorithm with a query complexity of $O(\log_2(N))$ [40]. However, for an unsorted database, the classical exhaustive search, also called brute-force (BF) search, with a query complexity of $O(N)$ has to be used. The worst-case scenario for the BF search implies that the desired element was found after N inspections. Although having the advantage of reducing the query complexity, quantum algorithms have a non-zero probability of failing [41], which has to be taken into considerations. The following subsections will detail the working principle and performance of the quantum algorithms that are relevant for the employed wireless decoders.

A. GROVER'S ALGORITHM

For an unsorted database, Grover's algorithm is capable of finding the index of a desired element, α_d, with a query complexity of only $O(\sqrt{N})$ [41]. Compared to the classical BF search, a square root improvement is achieved. To implement the Grover's QSA, the database size, N, and the number of existing solutions, S, that are equal to α_d must be known. The quantum circuit for Grover's QSA is shown in Fig. 11(a), where n qubits are initialized to the computational basis state $|0\rangle$. The $n = \lceil \log_2(N) \rceil$ qubits represent a register for holding the n-bits index of each element in the database. An n-qubits Hadamard transform is utilized to create a state with equal superposition as follows

$$|0\rangle^{\otimes n} \xrightarrow{H^{\otimes n}} \frac{1}{\sqrt{N}} \sum_{x=0}^{N-1} |x\rangle \equiv |\psi\rangle . \tag{16}$$

Then, an operation known as the Grover operator/iteration, G, is repeatedly applied, with the number of applications being $L = O(\sqrt{N/S})$. Thus, the existence of multiple solutions reduces the query complexity by a factor of $\sqrt{1/S}$. It turns out that the optimal number of Grover iterations is $L_{\text{opt}} = \lfloor 0.25\pi\sqrt{N/S} \rfloor$ [42]. The Grover operator G is depicted in Fig. 11(c), with the procedure applied as follows [13]:

Algorithm 1: Grover's QSA

```
Set the number of qubits n ← ⌈log2(N)⌉;
Initialize the n-qubits register to an equal superposition state |ψ⟩ = (1/√N) Σ_{x=0}^{N-1} |x⟩;
for i = 1 to ⌊0.25π√(N/S)⌋ do
    Apply the oracle, O;
    Apply Grover's diffusion operator, G = 2|ψ⟩⟨ψ| − I^{⊗n};
end
Measure the n-qubits register;
```

1) A quantum oracle, O, shifts the phase of the input state corresponding to the sought-after database element, α_d.
2) An n-qubits Hadamard transform, $H^{\otimes n}$, is applied.
3) A phase shift of -1 is applied to all of the states except for $|0\rangle$, which is expressed as

$$|x\rangle \rightarrow (-1)^{1-\delta_{x0}} |x\rangle , \quad \delta_{x0} = \begin{cases} 1 & x = 0, \\ 0 & x \neq 0, \end{cases} \tag{17}$$

with its unitary operator representation being

$$U_{\text{PS}} = 2|0\rangle^{\otimes n}\langle 0|^{\otimes n} - I^{\otimes n}. \tag{18}$$

4) A second $H^{\otimes n}$ is applied.

Thus, the Grover operator can be expressed as

$$\begin{aligned} G &= H^{\otimes n}\left(2|0\rangle^{\otimes n}\langle 0|^{\otimes n} - I^{\otimes n}\right)H^{\otimes n}O \\ &= \left(2H^{\otimes n}|0\rangle^{\otimes n}\langle 0|^{\otimes n}H^{\otimes n} - H^{\otimes n}I^{\otimes n}H^{\otimes n}\right)O \\ &= \left(2|\psi\rangle\langle\psi| - H^{\otimes n}H^{\otimes n}\right)O \\ &= \left(2|\psi\rangle\langle\psi| - I^{\otimes n}\right)O. \end{aligned} \tag{19}$$

The pseudocode of Grover's algorithm is shown in Algorithm 1. To elucidate the effect of Grover's iteration, define the non-solution and solution states, respectively, as

$$|\alpha\rangle \equiv \frac{1}{\sqrt{N-S}} \sum_{x \notin \text{Sol}} |x\rangle , \quad |\beta\rangle \equiv \frac{1}{\sqrt{S}} \sum_{x \in \text{Sol}} |x\rangle , \tag{20}$$

which are used to re-express the initial superposition state

$$|\psi\rangle = \sqrt{\frac{N-S}{N}}\,|\alpha\rangle + \sqrt{\frac{S}{N}}\,|\beta\rangle = \cos(\theta)\,|\alpha\rangle + \sin(\theta)\,|\beta\rangle , \tag{21}$$

where $\theta = \sin^{-1}(\sqrt{S/N})$ is the initial angle. The action of G in (19) can be demonstrated by considering the plane formed by defining $|\alpha\rangle$ and $|\beta\rangle$ to be the axes, as Fig. 11(c) shows. First, O performs a reflection about $|\alpha\rangle$. Then, $(2|\psi\rangle\langle\psi| - I^{\otimes n})$ performs a reflection about $|\psi\rangle$. Thus, G effectively rotates the starting vector, $|\psi\rangle$, towards $|\beta\rangle$. With each application of the Grover iteration subroutine, the amplitude of the states with an index corresponding to the desired α_d values increases, while the amplitude of other states decreases. After L_{opt} iterations of G, the measured state

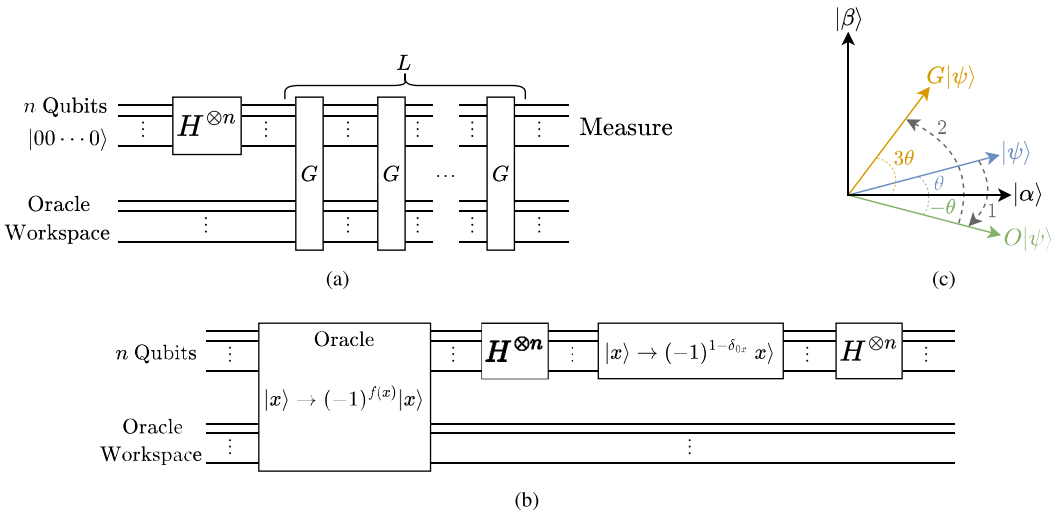

FIGURE 11. Quantum circuits for (a) Grover's algorithm, (b) the iteration *G*, and (c) the rotational effect of *G*.

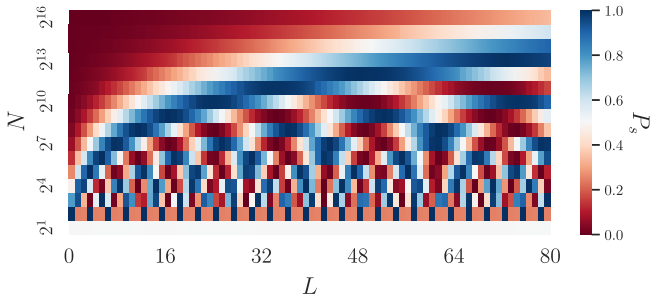

FIGURE 12. Grover's algorithm probability of success as a function *N* and *L*.

will return an index corresponding to α_d with near-absolute certainty. After L iterations, the resulting system state is [42]

$$G^L |\psi\rangle = \cos[(2L+1)\theta] |\alpha\rangle + \sin[(2L+1)\theta] |\beta\rangle . \quad (22)$$

The probability of success, P_s, is given by plugging the initial angle, θ, and the optimal number of Grover iterations, L_{opt}, into (22) and taking the complex magnitude of the second term

$$P_s = \sin^2\left[\left(2\left\lfloor 0.25\pi\sqrt{\frac{N}{S}}\right\rfloor + 1\right) \sin^{-1}\left(\sqrt{\frac{S}{N}}\right)\right]. \quad (23)$$

Fig. 12 shows the success probability dependence on N and L. Indicatively, the expression for L_{opt} traces the trajectory of most likely success.

B. BOYER-BRASSARD-HØYER-TAPP (BBHT) ALGORITHM

When only the desired element value, α_d, is known, but not its multiplicity, S, in an unsorted database, the BBHT QSA can be utilized [42]. Having less constraints while achieving the same end goal as that of Grover's QSA comes with added query complexity cost, which turns out to be no more than $4.5\sqrt{N}$ [43]. Thus, for a single existing solution, the complexity for both Grover's and BBHT QSAs is $O(\sqrt{N})$. Algorithm 2 describes the working principle of the BBHT QSA, involving multiple iterations of Grover's algorithm with additional classical steps.

Algorithm 2: BBHT QSA

1 Initialize $\lambda \in (1, 4/3)$, $m \leftarrow 1$, and $L_{\text{tot}} \leftarrow 0$;
2 Randomly choose $L \in \{0, 1, \ldots, \lfloor m \rfloor\}$;
3 Apply Algorithm 1 with L iterations of G, which outputs α_o;
4 Update $L_{\text{tot}} \leftarrow L_{\text{tot}} + L$;
5 **if** $\alpha_o = \alpha_d$ or $L_{\text{tot}} \geq \lceil 4.5\sqrt{N} \rceil$ **then**
6 | Return α_o;
7 **else**
8 | Update $m \leftarrow \min\left(\lambda m, \sqrt{N}\right)$;
9 | Go back to Line 2;
10 **end**

C. DÜRR-HØYER (DH) ALGORITHM

In the case where the desired element value, α_d, is unknown, the BBHT QSA cannot be used. When the desired element is the minimum value from the N-sized database, the DH QSA can be utilized [43], which is described in Algorithm 3. Similar to Grover's and BBHT QSAs, its query complexity is in the order of $O(\sqrt{N})$. Initially, the DH QSA picks a random element, i, from the database with value α_i. Then, it utilizes the BBHT QSA to find an element with a lower value. Then, the BBHT QSA is invoked again with the newly obtained lower value. As it turns out, the maximum number of Grover iterations is exactly five times that of the BBHT QSA [43].

Algorithm 3: DH QSA

Initialize $L_{\text{tot}} \leftarrow 0$;
Randomly choose an index $i \in \{0, 1, \ldots, N-1\}$;
Apply Algorithm 2 with the oracle marking all the indices, J, for which $\alpha_j < \alpha_i$, $\forall j \in J$, which entails L_{BBHT} iterations of G and outputs $\alpha_o = \alpha_j$, $j \in J$;
Update $L_{\text{tot}} \leftarrow L_{\text{tot}} + L_{\text{BBHT}}$;
if $\alpha_o \geq \alpha_i$ or $L_{\text{tot}} \geq \left\lceil 22.5\sqrt{N} \right\rceil$ **then**
    Return α_i;
else
    Update $\alpha_i \leftarrow \alpha_o$;
    Go back to Line 3;
end

TABLE 5. Constraints and query complexity of the discussed QSAs.

QSA	α_d	S	$\mathcal{Q}$
Grover's	Known	Known	$\left\lfloor 0.25\pi\sqrt{N/S} \right\rfloor$
BBHT	Known	Unknown	$\left\lceil 4.5\sqrt{N} \right\rceil$
DH	Unknown	Unknown	$\left\lceil 22.5\sqrt{N} \right\rceil$

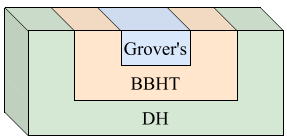

FIGURE 13. Illustration of the relation between the discussed QSAs.

D. QSA ASSESSMENT

The conditions for utilizing a QSA and the required number of Grover iterations are summarized in Table 5. Grover's algorithm lays at the heart of the BBHT and DH QSAs, while the remaining subroutines are purely classical as Fig. 13 depicts. Due to their probabilistic nature, the performance of the BBHT and DH QSAs is obtained by averaging many runs of the algorithm. The query complexity of each QSA and the linear classical BF search are shown in Fig. 14. The classical BF follows a perfect linear dependence, as already known. Grover's algorithm is always advantageous compared to all the remaining search methods. BBHT and DH start saving in query complexity over classical BF when the search space is greater than 23 and 509, respectively.

Similarly, Fig. 15 shows the failure probability, P_f, as a function of the search space size. Aside from the local ripples observed in the Grover's algorithm, the failure probability monotonically decreases as the search space increases, which aligns with the analytical analysis presented in [42]. On the other hand, the BBHT and DH QSAs start with a relatively high failure probability, which shortly reaches a minimum and then increases again until saturating at around 10^{-4} probability of failure. For BBHT and DH, two

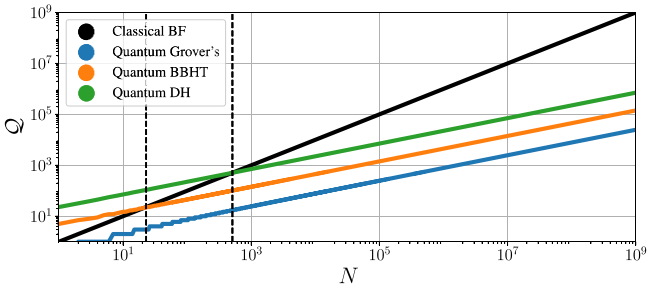

FIGURE 14. The query complexity as a function of N for each search algorithm.

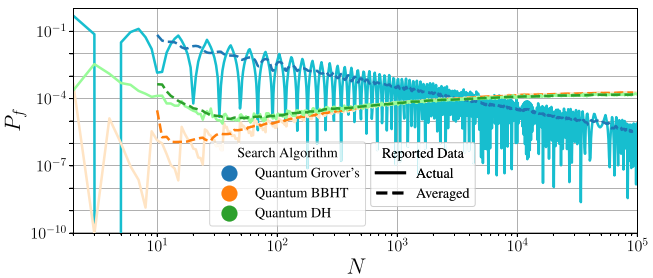

FIGURE 15. The failure probability, P_f, dependence on N. Solid lines represent the actual obtained performance, while the dashed curves are obtained using a moving average filter.

competing factors influence the probability of failure. At low N, the Grover's algorithm exhibits a high failure probability, as previously discussed. At high N, despite the Grover's algorithm having a low failure probability, its increased usage reduces the chance of successive successes. Therefore, a mid-range N represents the optimal trade-off between these extremes.

E. QUANTUM SORTING ALGORITHM

The daunting task of database sorting has been subject to much research [44]. For a given N, there are $N!$ possible orderings for its elements. The best-performing algorithms entail a query complexity of $O(N\log_2(N))$ [32], where the exact value depends on the utilized algorithm and nature of the data. Fundamental to many sorting algorithms is the compare-and-swap operation [45]. For an error-free comparison-based quantum sorting algorithm, the theoretical lower bound on its query complexity is [33]

$$\mathcal{Q}_{\text{QS}}(N) = \frac{N}{2\pi}\left(\sum_{i=1}^{N}\frac{1}{i} - 1\right) \approx 0.11N\log_2(N), \quad (24)$$

which is a constant factor better than state-of-the-art classical sorting algorithms. Thus, unlike the minimum-finding problem, quantum computers are not significantly better than classical ones for the sorting problem.

VI. QUANTUM-ASSISTED DECODERS: ANALYSIS AND ASSESSMENT

Having covered the relevant quantum algorithms, this section investigates their impact on the query complexity and performance of the decoders discussed in Section III. Specifically, the effects on different transmission schemes

(i.e., diversity, spatial modulation, and multiplexing) are examined. The objective is to determine the extent to which these decoders can leverage quantum algorithms to improve performance under various system parameters and transmission schemes. To achieve this, mathematical analysis and Monte Carlo simulations are performed.

A. PROBABILITY OF ERROR ANALYSIS

In conventional decoders, signal decoding is performed by computing the likelihood of various transmission scenarios and selecting the one that minimizes the error function. The success of the latter step, which involves finding the global minimum error among a large set of real-valued error values, is ensured in classical signal decoding. In contrast, while the DH QSA generally reduces the necessary query complexity, it introduces a slight risk of failing to identify the global minimum solution. The signal is correctly decoded when the global minimum error computed by the decoder corresponds to the true signal and is successfully obtained by the DH QSA. However, even if the global minimum error does not correspond to the true signal, there remains a non-zero probability that the DH QSA might coincidentally choose the correct solution if it fails (e.g., second minimum). Considering these two scenarios, the probability of correctly classifying the symbol using the DH QSA is given by

$$P_s^q = \left(1 - P_e^c\right)\left(1 - P_f^d\right) + \frac{P_e^c P_f^d}{|\mathcal{S}| - 1}, \tag{25}$$

where P_e^c is the classical decoder symbol error rate (SER), P_f^d is the DH QSA failure probability, and $|\mathcal{S}|$ is the search space size, which depends on the utilized decoding algorithm as

$$|\mathcal{S}| = \begin{cases} |\mathcal{P}| & \text{RB/ML,} \\ C & \text{CB/CRB/RCB,} \\ MK & \text{KB,} \end{cases} \tag{26}$$

where $|\mathcal{P}|$ is given by (3). The first term in (25) represents the scenario where both the classical decoder and DH QSA succeed. Conversely, the second term accounts for the situation when both fail, yet there remains a small probability that the correct symbol is coincidentally chosen by the DH QSA. Utilizing (25), the SER of a quantum-assisted decoder is derived as follows

$$\begin{aligned} P_e^q &= 1 - P_s^q = P_e^c + P_f^d - P_e^c P_f^d \left(1 + \frac{1}{|\mathcal{S}| - 1}\right) \\ &= P_e^c + P_f^d \alpha, \quad \alpha \equiv 1 - P_e^c \frac{|\mathcal{S}|}{|\mathcal{S}| - 1} \in [-1, 1], \end{aligned} \tag{27}$$

where $\alpha = -1$ occurs in the extreme case when $P_e^c = 1$ and $|S| = 2$, resulting in $P_e^q = 1 - P_f^d$. Conversely, $P_e^c = 0$ results in $\alpha = -1$, leading to $P_e^q = P_f^d$. This indicates that when the total signal-to-noise ratio (SNR)[2] is high, P_e^c diminishes

[2]The total SNR considers the total signal power before being divided among the Tx antennas. Its relation to the SNR per channel, SNR_c, is

$$\text{SNR}_\text{c} = \text{SNR} - 10\log_{10}(N_t).$$

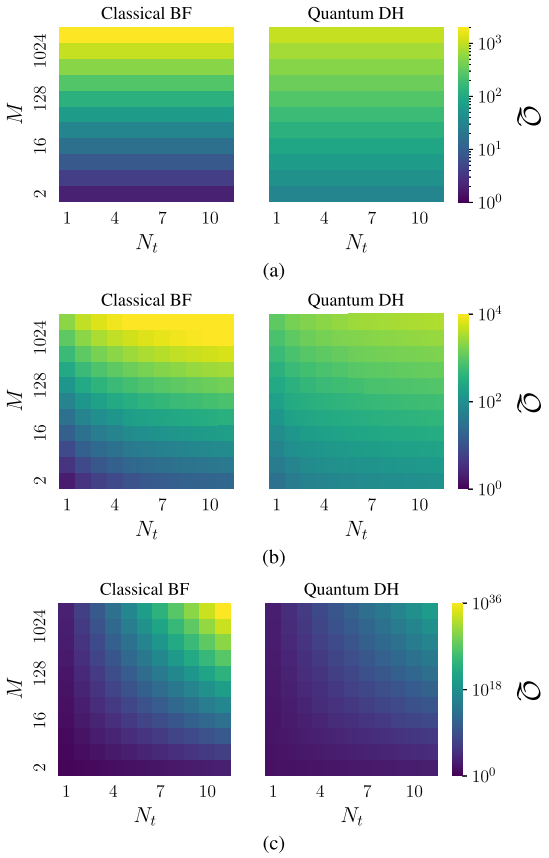

FIGURE 16. Effect of varying the modulation order, M, and Tx antennas, N_t, on the query complexity for the (a) diversity, (b) spatial modulation, and (c) multiplexing systems.

and thus P_f^d dominates in (27), resulting in an SER floor that is approximated by

$$\text{SER}_\text{min} \approx P_f^d. \tag{28}$$

Moreover, when assuming a Gray coding in the high-SNR regime, the approximate bit error rate (BER) floor is [46]

$$\text{BER}_\text{min} \approx \frac{\text{SER}_\text{min}}{\log_2(M)}. \tag{29}$$

In practical communication systems, a maximum value for the uncoded BER is tolerated, which is the predefined BER threshold, BER_t. The BER_t reflects the desired data transmission quality, so the DH QSA can be used as long as $\text{BER}_\text{min} \leq \text{BER}_t$ is satisfied in the high-SNR regime.

B. QUANTUM-ASSISTED ML

Utilizing the DH QSA to search for the minimum among all the computed possibilities of (4) significantly alters the original BF query complexity. This change is illustrated in Fig. 16, which shows the query complexity for the various transmission schemes as a function of the number of Tx antennas and modulation order. As analyzed in Section V, a search space that is too small (≤ 509) actually leads to worse query complexity for the DH QSA. This is particularly evident when $M \leq 4$. Conversely, the DH QSA is more

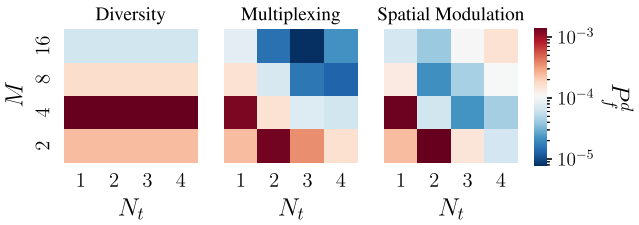

FIGURE 17. The failure probability of DH QSA as a function of M and N_t for the ML decoder.

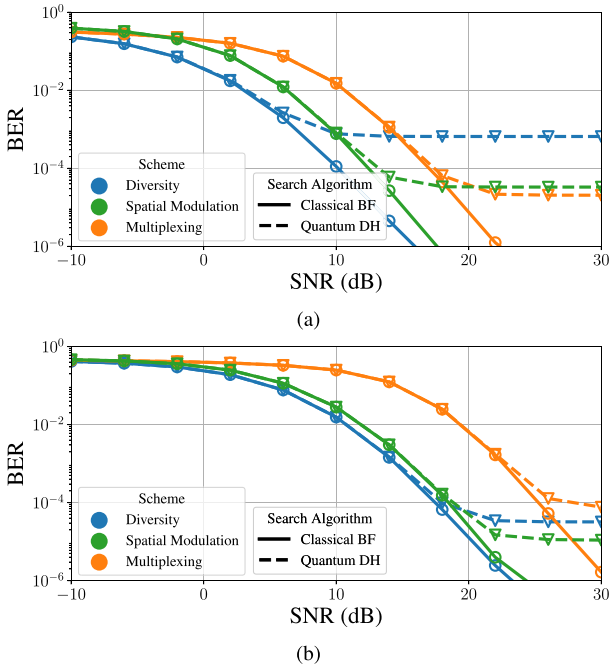

FIGURE 18. ML decoder BER vs. SNR performance with $N_t = N_r = 4$ for (a) $M = 4$ and (b) $M = 16$.

advantageous when M is larger. For the diversity scheme, when $M = 512$, classical BF and quantum DH result in almost the same query complexity, since the search space is close to the 509 threshold. However, for the spatial modulation scheme, a reduction in query complexity is achieved when $N_t \geq 2$. A substantial reduction in the query complexity is observed for the multiplexing scheme, as its search space scales exponentially with N_t.

The performance of the quantum-assisted ML decoder depends on the system's search space size. The relation between the transmission parameters and failure probability is shown in Fig. 17. The quantum algorithm success probability is relatively low when the search space is too small, as is the case for $M \leq 8$ in the diversity scheme. Similarly, a search space that is too big, such as the multiplexing case for $M = 16$ and $N_t = 4$, will have a low probability of success. The considered range of M and N_t results in the spatial modulation scheme being the most compatible with the DH QSA since its search space scales as MN_t, which tends to be in the middle sweet spot of Fig. 15.

TABLE 6. The query complexity of the FCSD algorithms where the scheme parameters are $C = 48$ for the diversity, $C = 1{,}536$ for the spatial modulation, and $K = 128$ for the multiplexing.

Scheme	Algorithm	Classical $\mathcal{Q}$	Quantum $\mathcal{Q}$	% Reduction
Diversity	RB	64	180	−181.3%
	CB/CRB/RCB	406	194	52.2%
Spatial Modulation	RB	2,048	1,019	50.2%
	CB/CRB/RCB	23,215	3,367	85.5%
Multiplexing	KB	1,728,512	337,955	80.5%

To obtain the SER of the quantum-assisted ML decoder, (27) is utilized after computing P_f^d and $|\mathcal{S}|$ for the specific system parameters. The BER dependence on the total SNR is plotted in Fig. 18. For $M = 4$, the diversity scheme exhibits a higher BER_{min} due to the extremely small search space. Conversely, for $M = 16$, the multiplexing scheme has a high BER_{min} because of the extremely large search space. On the other hand, the quantum-assisted spatial modulation system demonstrates a more robust BER_{min} performance for both modulation orders. The usability of quantum-assisted decoders depends on the required performance. For instance, a realistic threshold for the uncoded BER in wireless communication is $\text{BER}_t = 10^{-4}$ [47]. This threshold is met by all the scenarios shown in Fig. 18, except for the diversity scheme with $M = 4$.

C. QUANTUM-ASSISTED FCSD

A practical alternative to the high computational complexity ML decoder is the FCSD algorithm. The two stages of the FCSD algorithm, which involve sorting and determining the minimum element, can be augmented with quantum algorithms to reduce the query complexity. Considering the system parameters $M = 64$ and $N_t = N_r = 32$ for the three transmission schemes (i.e., diversity, spatial modulation, and multiplexing), Table 6 compares the classical and quantum query complexities for all the tree algorithms. The tree parameters are $C = 48$ and $C = 1{,}536$ for the diversity and spatial modulation schemes, respectively, corresponding to expanding three-fourths of the branches. For the multiplexing scheme, $K = 128$ is chosen. The percent reduction is defined as

$$\%\ \text{Reduction} = \frac{\text{Classical } \mathcal{Q} - \text{Quantum } \mathcal{Q}}{\text{Classical } \mathcal{Q}} \times 100. \quad (30)$$

Aside from the diversity scheme with the RB algorithm, utilizing the DH QSA and theoretical quantum sort significantly reduces query complexity, especially for the two-stage (i.e., CB, CRB, and RCB) and KB algorithms in the spatial modulation and multiplexing schemes, respectively. Consistent with previous findings, the RB algorithm with the diversity scheme, which does not require a sorting algorithm, generally results in a higher query complexity for the quantum-augmented decoder.

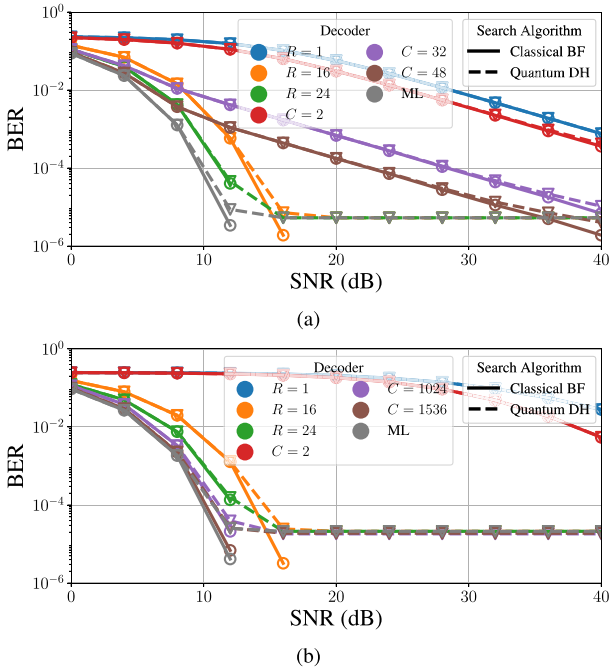

FIGURE 19. RB and CB algorithms BER vs. SNR performance with $M = 64$ and $N_t = N_r = 32$ for the (a) diversity and (b) spatial modulation schemes.

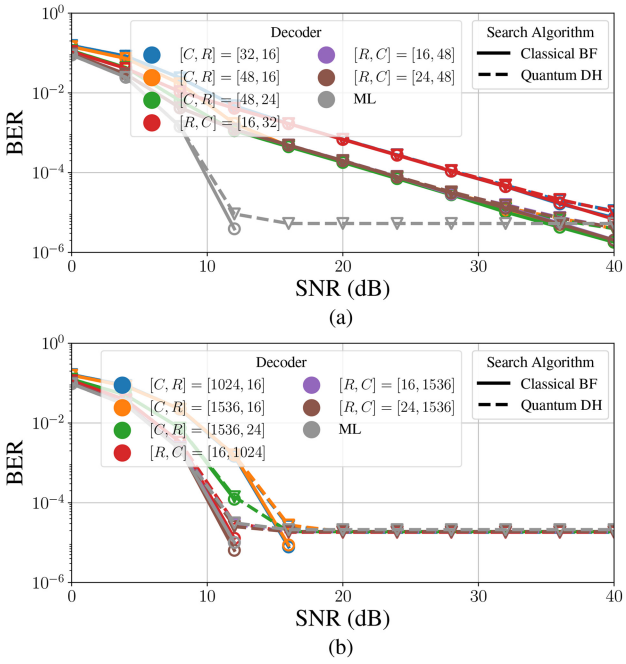

FIGURE 20. BER vs. SNR of the CRB and RCB algorithms with $M = 64$ and $N_t = N_r = 32$ for the (a) diversity and (b) spatial modulation schemes.

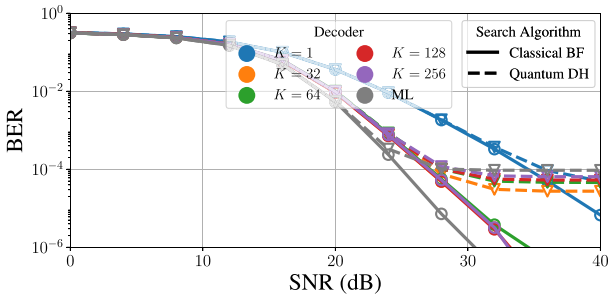

FIGURE 21. BER performance of the KB algorithm as a function of the SNR for $M = 16$ and $N_t = N_r = 4$.

The BER dependence on the SNR for the RB and CB algorithms is shown in Fig. 19. Opting for an extremely minimal decoder (e.g., $R = 1$ or $C = 2$) adversely affects the BER, which conceals the suboptimal performance of the DH QSA when the search space is very small (e.g., $C = 2$). For $C = 32$ and $C = 48$ in Fig. 19, the performance saturation due to the DH QSA is evident in the high-SNR regime. For the RB and ML decoders, the search space is constant, which is 64 and 2,048 for the diversity and spatial modulation schemes, respectively. Noting Fig. 15, the expected saturation levels for the RB and ML decoders are comparable, which agrees with Fig. 19, where the diversity scheme has a slightly better performance due to the chosen modulation order. Fig. 20 shows a similar behavior for the CRB and RCB methods, where the quantum-assisted decoders saturate at around BER $= 10^{-5}$.

For the multiplexing scheme, Fig. 21 shows the BER performance of the KB algorithm. The ML decoder has the highest BER floor due to its larger search space. For the same reason, higher values of K result in an earlier performance saturation. However, when K becomes too small, as is the case when $K = 1$, the performance is again suboptimal. The best performance is obtained when $K = 32$, corresponding to a search space of size 512. Thus, the KB method is capable of outperforming the ML decoder in the high-SNR regime while saving in both computational and query complexities.

Considering the system parameters $4 \leq M \leq 1{,}024$ and $1 \leq N_t \leq 3$ for $\text{BER}_t = 1.6 \times 10^{-5}$, some deductions can be made about the efficiency of quantum algorithms with the ML and RB decoders. For the diversity scheme, quantum algorithms are inefficient due to the limited search space, leading to increased query complexity for most cases ($M \leq 256$). In contrast, spatial modulation and multiplexing schemes show significant query complexity reduction across a broader range of system complexities. From (29), maintaining $\text{BER}_{\min} \leq \text{BER}_t$ depends on P_f^d and M, where the former has a direct relation to N which is captured by Fig. 15. For the diversity and spatial modulation schemes, $\text{BER}_{\min} \leq \text{BER}_t$ is satisfied when $M \geq 32$ and $MN_t \geq 24$, respectively. On the other hand, the threshold BER is satisfied for the multiplexing scheme when $32 \leq M^{N_t} \leq 1{,}024$ or $M^{N_t} \geq 1{,}048{,}576$. These findings are illustrated in Fig. 22, where the spatial modulation scheme is shown to be the most applicable considering both $\mathcal{Q}$ and BER. In a practical communication scenario with known requirements and fixed system parameters, the decision on whether to use quantum computing for signal decoding is guided by Fig. 22. If different parameters are of interest, the corresponding performance is analyzed in a similar manner.

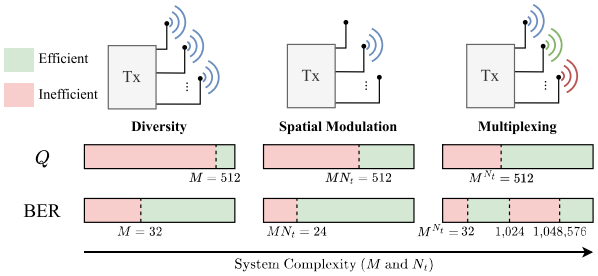

FIGURE 22. Applicability of quantum algorithms in signal decoding for the different considered communication systems and scenarios.

VII. CONCLUSION

This paper assessed the applicability of quantum algorithms in solving the decoding problem in wireless communication. The DH and optimal sorting quantum algorithms were applied to various operational scenarios for MIMO system decoding. These quantum algorithms can reduce the number of required queries for decoding compared to classical methods. The non-ideal performance of the DH QSA and its dependence on the search space size were analyzed, which translated into its applicability to the considered MIMO systems. It was found that the quantum algorithms are unsuitable for the diversity scheme due to the small search space, which lowers the performance of the DH QSA with little or no reduction in the query complexity. On the other hand, assuming a non-minimal FCSD implementation, the quantum algorithms are generally applicable to both decoders in the spatial modulation and multiplexing schemes. Higher query complexity savings are obtained for the ML decoder in these cases. Overall, the usability of quantum algorithms will depend on the specific requirements of the utilized system (e.g., BER_t) and the chosen parameters (e.g., M and N_t). Considering other communication systems in future work would be beneficial in further exploring the applicability of quantum computing in signal decoding. This study paves the way for an appropriate methodology to follow when quantum algorithms are considered for use in wireless communication system decoding.

REFERENCES

[1] H. Lu et al., "A tutorial on near-field XL-MIMO communications towards 6G," *IEEE Commun. Surveys Tuts.*, early access, Apr. 12, 2024, doi: 10.1109/COMST.2024.3387749.

[2] Z. Wang et al., "A tutorial on extremely large-scale MIMO for 6G: Fundamentals, signal processing, and applications," *IEEE Commun. Surveys Tuts.*, vol. 26, no. 3, pp. 1560–1605, 3rd Quart., 2024, doi: 10.1109/COMST.2023.3349276.

[3] M. Cui, Z. Wu, Y. Lu, X. Wei, and L. Dai, "Near-field MIMO communications for 6G: Fundamentals, challenges, potentials, and future directions," *IEEE Commun. Mag.*, vol. 61, no. 1, pp. 40–46, Jan. 2023.

[4] A. J. Paulraj, D. A. Gore, R. U. Nabar, and H. Bolcskei, "An overview of MIMO communications—A key to gigabit wireless," *Proc. IEEE*, vol. 92, no. 2, pp. 198–218, Feb. 2004.

[5] J. Nam, G. Caire, and J. Ha, "On the role of transmit correlation diversity in multiuser MIMO systems," *IEEE Trans. Inf. Theory*, vol. 63, no. 1, pp. 336–354, Jan. 2017.

[6] G. Bartoli, A. Abrardo, N. Decarli, D. Dardari, and M. Di Renzo, "Spatial multiplexing in near field MIMO channels with reconfigurable intelligent surfaces," *IET Signal Process.*, vol. 17, no. 3, Mar. 2023, Art. no. e12195.

[7] R. Y. Mesleh, H. Haas, S. Sinanovic, C. W. Ahn, and S. Yun, "Spatial modulation," *IEEE Trans. Veh. Technol.*, vol. 57, no. 4, pp. 2228–2241, Jul. 2008.

[8] L. He, L. Fan, X. Lei, X. Tang, P. Fan, and A. Nallanathan, "Learning-based MIMO detection with dynamic spatial modulation," *IEEE Trans. Cogn. Commun. Netw.*, vol. 9, no. 6, pp. 1489–1502, Dec. 2023.

[9] X. Zhu and R. D. Murch, "Performance analysis of maximum likelihood detection in a MIMO antenna system," *IEEE Trans. Commun.*, vol. 50, no. 2, pp. 187–191, Feb. 2002.

[10] C.-X. Wang et al., "On the road to 6G: Visions, requirements, key technologies, and testbeds," *IEEE Commun. Surveys Tuts.*, vol. 25, no. 2, pp. 905–974, 2nd Quart., 2023.

[11] C. Wang and A. Rahman, "Quantum-enabled 6G wireless networks: Opportunities and challenges," *IEEE Wireless Commun.*, vol. 29, no. 1, pp. 58–69, Feb. 2022.

[12] A. Montanaro, "Quantum algorithms: An overview," *NPJ Quantum Inf.*, vol. 2, no. 1, pp. 1–8, Jan. 2016.

[13] M. A. Nielsen and I. L. Chuang, *Quantum Computation and Quantum Information*. Cambridge, U.K.: Cambridge Univ. Press, 2000.

[14] P. W. Shor, "Algorithms for quantum computation: Discrete logarithms and factoring," in *Proc. 35th Annu. Symp. Found. Comput. Sci.*, 1994, pp. 124–134.

[15] M. Kim, S. Kasi, P. A. Lott, D. Venturelli, J. Kaewell, and K. Jamieson, "Heuristic quantum optimization for 6G wireless communications," *IEEE Netw.*, vol. 35, no. 4, pp. 8–15, Jul./Aug. 2021.

[16] B. Narottama and S. Y. Shin, "Quantum neural networks for resource allocation in wireless communications," *IEEE Trans. Wireless Commun.*, vol. 21, no. 2, pp. 1103–1116, Feb. 2022.

[17] P. Botsinis et al., "Quantum search algorithms for wireless communications," *IEEE Commun. Surveys Tuts.*, vol. 21, no. 2, pp. 1209–1242, 2nd Quart., 2019.

[18] P. Botsinis et al., "Quantum-assisted indoor localization for uplink mm-Wave and downlink visible light communication systems," *IEEE Access*, vol. 5, pp. 23327–23351, 2017.

[19] S. Mondal, M. R. Laskar, and A. K. Dutta, "ML criterion based signal detection of a MIMO-OFDM system using quantum and semi-quantum assisted modified DHA/BBHT search algorithm," *IEEE Trans. Veh. Technol.*, vol. 70, no. 2, pp. 1688–1698, Feb. 2021.

[20] P. Botsinis, D. Alanis, Z. Babar, S. X. Ng, and L. Hanzo, "Joint quantum-assisted channel estimation and data detection," *IEEE Access*, vol. 4, pp. 7658–7681, 2016.

[21] P. Botsinis et al., "Quantum-aided multi-user transmission in non-orthogonal multiple access systems," *IEEE Access*, vol. 4, pp. 7402–7424, 2016.

[22] P. Botsinis, D. Alanis, Z. Babar, S. X. Ng, and L. Hanzo, "Iterative quantum-assisted multi-user detection for multi-carrier interleave division multiple access systems," *IEEE Trans. Commun.*, vol. 63, no. 10, pp. 3713–3727, Oct. 2015.

[23] P. Botsinis, S. X. Ng, and L. Hanzo, "Fixed-complexity quantum-assisted multi-user detection for CDMA and SDMA," *IEEE Trans. Commun.*, vol. 62, no. 3, pp. 990–1000, Mar. 2014.

[24] P. Botsinis, S. X. Ng, and L. Hanzo, "Quantum search algorithms, quantum wireless, and a low-complexity maximum likelihood iterative quantum multi-user detector design," *IEEE Access*, vol. 1, pp. 94–122, 2013.

[25] I. Al-Nahhal, E. Basar, O. A. Dobre, and S. Ikki, "Optimum low-complexity decoder for spatial modulation," *IEEE J. Sel. Areas Commun.*, vol. 37, no. 9, pp. 2001–2013, Sep. 2019.

[26] K.-w. Wong, C.-Y. Tsui, R. S.-K. Cheng, and W.-H. Mow, "A VLSI architecture of a K-best lattice decoding algorithm for MIMO channels," in *Proc. IEEE Int. Symp. Circuits Syst. (ISCAS)*, 2002, pp. 273–276.

[27] L. G. Barbero and J. S. Thompson, "Fixing the complexity of the sphere decoder for MIMO detection," *IEEE Trans. Wireless Commun.*, vol. 7, no. 6, pp. 2131–2142, Jun. 2008.

[28] I. Al-Nahhal, O. A. Dobre, and S. Ikki, "Low complexity decoders for spatial and quadrature spatial modulations—Invited paper," in *Proc. IEEE 87th Veh. Technol. Conf. (VTC)*, 2018, pp. 1–5.

[29] I. Al-Nahhal, A. Emran, H. Kasem, A. B. A. El-Rahman, O. Muta, and H. Furukawa, "Flexible fractional K-best sphere decoding for uncoded MIMO channels," *IEICE Commun. Exp.*, vol. 4, no. 1, pp. 20–25, Jan. 2015.
[30] H. Buhrman and R. de Wolf, "Complexity measures and decision tree complexity: A survey," *Theor. Comput. Sci.*, vol. 288, no. 1, pp. 21–43, Oct. 2002.
[31] S. Bubeck, "Convex optimization: Algorithms and complexity," *Found. Trends® Mach. Learn.*, vol. 8, nos. 3–4, pp. 231–357, Nov. 2015.
[32] A. Zutshi and D. Goswami, "Systematic review and exploration of new avenues for sorting algorithm," *Int. J. Inf. Manage. Data Insights*, vol. 1, no. 2, Nov. 2021, Art. no. 100042.
[33] P. Høyer, J. Neerbek, and Y. Shi, "Quantum complexities of ordered searching, sorting, and element distinctness," *Algorithmica*, vol. 34, no. 4, pp. 429–448, Nov. 2002.
[34] "Partial sort—C++ reference." cppreference.com. Accessed: Jul. 11, 2024. [Online]. Available: https://en.cppreference.com/w/cpp/algorithm/partial_sort
[35] M. R. Garey, D. S. Johnson, and L. Stockmeyer, "Some simplified NP-complete graph problems," *Theor. Comput. Sci.*, vol. 1, no. 3, pp. 237–267, Feb. 1976.
[36] J. R. Powell, "The quantum limit to Moore's law," *Proc. IEEE*, vol. 96, no. 8, pp. 1247–1248, Aug. 2008.
[37] P. A. M. Dirac, *The Principles of Quantum Mechanics*. Oxford, U.K.: Oxford Univ. Press, 1981.
[38] R. Horodecki, P. Horodecki, M. Horodecki, and K. Horodecki, "Quantum entanglement," *Rev. Mod. Phys.*, vol. 81, pp. 865–942, Jun. 2009.
[39] S. Aaronson, "The limits of quantum," *Sci. Am.*, vol. 298, no. 3, pp. 62–69, Mar. 2008.
[40] J. L. Bentley, "Multidimensional binary search trees used for associative searching," *Commun. ACM*, vol. 18, no. 9, pp. 509–517, Sep. 1975.
[41] L. K. Grover, "A fast quantum mechanical algorithm for database search," in *Proc. 28th Annu. ACM Symp. Theory Comput.*, 1996, pp. 212–219.
[42] M. Boyer, G. Brassard, P. Høyer, and A. Tapp, "Tight bounds on quantum searching," *Fortschritte der Physik*, vol. 46, nos. 4–5, pp. 493–505, Apr. 1998.
[43] C. Dürr and P. Høyer, "A quantum algorithm for finding the minimum," 1996, *arXiv:quant-ph/9607014*.
[44] D. E. Knuth, *The Art of Computer Programming*, vol. 3, London, U.K.: Pearson Educ., 1997.
[45] S. G. Akl, *Parallel Sorting Algorithms*, vol. 12, Cambridge, MA, USA: Academic, 2014.
[46] J. G. Proakis, M. Salehi, N. Zhou, and X. Li, *Communication Systems Engineering*, vol. 2, Hoboken, NJ, USA: Prentice-Hall, 1994.
[47] T. S. Rappaport, *Wireless Communications: Principles and Practice*. Cambridge, U.K.: Cambridge Univ. Press, 2024.